IEEE Access
Multidisciplinary | Rapid Review | Open Access Journal

Received July 21, 2020, accepted August 1, 2020, date of publication August 5, 2020, date of current version September 9, 2020.

Digital Object Identifier 10.1109/ACCESS.2020.3014421

Reconfigurable Optical Frequency Comb and Nyquist Pulses Generation With Tunable Sensitivities

HONGYAO CHEN[1], JIANPING WANG[1], HUIMIN LU[1], TIGANG NING[2], LI PEI[2], AND JING LI[2], (Member, IEEE)

[1]School of Computer and Communication Engineering, University of Science and Technology Beijing, Beijing 100091, China
[2]Key Laboratory of All Optical Network and Advanced Telecommunication Network of EMC, Institute of Lightwave Technology, Beijing Jiaotong University, Beijing 100044, China

Corresponding author: Hongyao Chen (chenhongyao@ustb.edu.cn)

This work was supported in part by the China Postdoctoral Science Foundation under Grant 2019M660461, and in part by the Fundamental Research Funds for the Central Universities under Grant FRF-TP-18-059A1 and Grant FRF-BD-20-11A.

ABSTRACT In this paper, a practical scheme to achieve reconfigurable optical frequency comb (OFC) and Nyquist pulses generation based on two cascaded Mach–Zehnder modulators and a polarization control structure is theoretically analyzed and verified by simulation. A rectangular-shaped OFC with evolvable comb lines (4 to 8) was obtained. Since there is no filter built in the structure, the turntable comb spacing is also an inherent feature of the OFC. These properties make the OFC can be used to produce high quality Nyquist pulses with flexible pulse duration (25.6ps∼14.4ps), duty cycle (11.5%∼20.5%) and repetition rate (4GHz∼40GHz). It is found that the sensitivity of the reconstruction process of the OFC and corresponding pulses is adjustable. By methods of mathematics, we expound the observed results and provide mathematical expressions about the relations between the optical sideband suppression ratio, modulation index, principle polarization direction and sensitivity. Moreover, a proof-of-concept experiment of the OFC generation is carried out and the results are consistent with the theoretical ones, which indicates the potential of our work to generate user-friendly reconfigurable OFC and Nyquist pulses demanded in microwave photonics, optical communications, all-optical sampling and light storage applications.

INDEX TERMS Microwave photonics, optical harmonic generation, optical pulses generation.

I. INTRODUCTION

A phase-locked and rectangular-shaped optical frequency comb (OFC) has a sinc-shaped pulse envelope in time domain, which is known as optical sinc-shaped Nyquist pulses [1]. Optical sinc-shaped Nyquist pulses are of particular interest to scholars in the field of optical communication, because they are satisfying the Nyquist criterion of zero inter-symbol interference (ISI), enabling data to be encoded with a minimum spectral bandwidth and have a better tolerance to nonlinear impairment and fiber dispersion [2], [3]. In future optical networks, it is crucial to develop all-optical signal sampling and processing to avoid the limits of electronic bottlenecks. Sinc-shaped Nyquist pulses are also considered as promising candidates for the future photonic analog-to-digital conversion [4] and microwave filtering devices [5] due to them temporal and spectral features, such as multi-wavelength operation, tunable repetition rate and corresponding to the ideal interpolation function. Besides the above applications, the high quality and flexibility of the sinc-shaped Nyquist pulses can bring benefits to many other fields, such as integrated optics [3], [6], spectroscopy [7] and light storage [8], [9].

The generation of optical Nyquist pulses can be achieved by using pulse shaping [10] or parametric amplification [11], [12], but most of the methods reported so far have remained with higher roll-off factor and none has led to ideal sinc-shaped pulses. Reference [1] shows a method to produce sinc-shaped Nyquist pulses of very high quality. It is based on the direct synthesis of a rectangular-shaped and phase-locked frequency comb and the comb can be easily achieved by using a simple external modulation structure. Thus, several approaches to generate a sequence of high-quality Nyquist pulses based on external modulators have been proposed for their advantages of almost ideal rectangular spectrum, negligible roll-off factor, tunability of repetition rate and simple

The associate editor coordinating the review of this manuscript and approving it for publication was Bilal Khawaja.

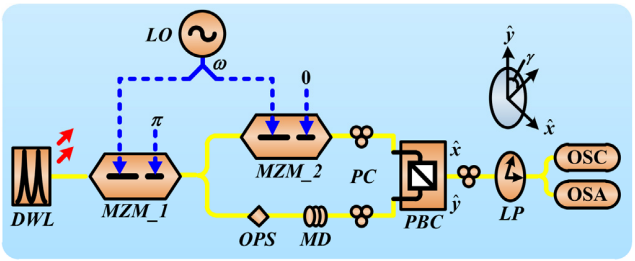

FIGURE 1. The schematic diagram of the proposed reconfigurable OFC and Nyquist pulses generator (DWL, dual-wavelength laser; OPS, optical phase shifter; LO, local oscillator; MD, matching delay; PBC, polarization beam combiner; LP, linear polarizer; MZM, Mach-Zehnder modulator; PC, polarization controller; OSC, oscilloscope; OSA, optical spectrum analyzer).

configuration [13]–[18]. Recently, some scholars began to pay attention to achieve the approaches with CMOS technologies, for example, an integrated 9-lines-OFC and Nyquist pulses generation has been demonstrated by using two cascaded silicon Mach-Zehnder Modulators (MZMs) [3], which indicates the OFC and Nyquist pulses generation technique has a potential application for the integrated microwave photonics system.

Though these schemes have itself advantages, they have shortcomings in flexibility and reconfiguration, such as the final pulses cannot be reconstructed completely, especially the pulse duty cycle is usually fixed and even if the scheme has the characteristic of reconstruction, the key often lies in the change of input carrier number or modulation index of the used modulator, which cannot realize the continuous change of duty cycle of the pulses, let alone the adjustable reconstruction sensitivity [19], [20]. In this work, a method to generate OFC and Nyquist pulses with complete reconstruction characteristics is proposed and theoretically analyzed. A flexible OFC with an almost ideal and evolvable rectangular spectrum was obtained, which can be used to produce reconfigurable Nyquist pulses. The pulses have possessed the sinc-shape and a series of dynamic characteristics, such as a tunable duty cycle of 9%, a variable repetition rate and adjustable pulse duration. Moreover, a varied sensitivity can be used, in the scheme, to control the reconstruction process and makes our design more flexible and adaptive to changes.

II. PRINCIPLE AND THEORETICAL ANALYSIS

The schematic diagram of the proposal is shown in Fig.1. The input optical field is generated by a dual-wavelength laser (DWL). When the frequency interval between the two optical carriers is equal to the electrical driving signal's frequency, the optical field can be assumed as

$$E_{in}(t) = E_0 \{\exp(j2\pi f_0 t) + \exp[j2\pi (f_0 + f_m) t]\}. \quad (1)$$

where f_0 and $f_0 + f_m$ denote the center frequency of the two optical carriers, E_0 represents the amplitude of the optical field and f_m symbolize the output frequency of the local oscillator (LO). For high stability of the final pulse train, the phase fluctuations of the two carriers should be correlated, therefore, the phase noise terms are not shown in (1). The electrical driving signal is divided into two paths to drive the two Mach-Zehnder modulators, MZM_1 and MZM_2. Since MZM_1 is biased at the minimum transmission point, the output optical field of MZM_1 can be expressed as

$$E_{MZM\_1}(t) = E_0 \sum_{n=1}^{\infty} (-1)^n J_{2n-1}(m) \begin{Bmatrix} \exp[j2\pi (f_0 - (2n-1) f_m) t] \\ + \exp[j2\pi (f_0 + (2n-1) f_m) t] \\ + \exp[j2\pi (f_0 - (2n-2) f_m) t] \\ + \exp[j2\pi (f_0 + 2n f_m) t] \end{Bmatrix}. \quad (2)$$

where J_n denotes the Bessel function of the first kind of order n. m is the modulation index (MI) of MZM_1. When m equals to 0.8, the corresponding values of $J_1(m)$, $J_3(m)$, $J_5(m)$ and $J_7(m)$ are 0.3688, 0.0102, 8.3084×10^{-5} and 3.1864×10^{-7}, respectively. Thus, the optical sidebands higher than $\pm 3^{rd}$, can be neglected without significant errors, and the E_{MZM_1} can be simplified to

$$E_{MZM\_1}(t) = -E_0 J_1(m) \cdot \begin{Bmatrix} \exp[j2\pi (f_0 - f_m) t] \\ + \exp[j2\pi (f_0 + f_m) t] \\ + \exp[j2\pi (f_0) t] \\ + \exp[j2\pi (f_0 + 2f_m) t] \end{Bmatrix} + E_0 J_3(m) \cdot \begin{Bmatrix} \exp[j2\pi (f_0 - 3f_m) t] \\ + \exp[j2\pi (f_0 - 2f_m) t] \\ + \exp[j2\pi (f_0 + 3f_m) t] \\ + \exp[j2\pi (f_0 + 4f_m) t] \end{Bmatrix}. \quad (3)$$

Then the output signal will be divided into two parts: one is modulated by MZM_2; the other achieves phase reversal via an optical phase shifter (OPS). As $J_3(m)$ is much smaller than $J_1(m)$, we can consider that only the four strong frequency components are affected by MZM_2. When MZM_2 operates in weak modulation state (MI, $\beta = 0.58$) and is based at the maximum transmission point, the output optical field of MZM_2 can be written as

$$E_{MZM\_2}(t) = +\frac{1}{\sqrt{2}} E_0 \cdot \begin{bmatrix} J_3(m) \\ +J_1(m) J_2(\beta) \end{bmatrix} \cdot \begin{Bmatrix} \exp[j2\pi (f_0 - 3f_m) t] \\ + \exp[j2\pi (f_0 - 2f_m) t] \\ + \exp[j2\pi (f_0 + 3f_m) t] \\ + \exp[j2\pi (f_0 + 4f_m) t] \end{Bmatrix} - \frac{1}{\sqrt{2}} E_0 \cdot \begin{bmatrix} J_1(m) J_0(\beta) \\ -J_1(m) J_2(\beta) \end{bmatrix} \cdot \begin{Bmatrix} \exp[j2\pi (f_0 - f_m) t] \\ + \exp[j2\pi (f_0) t] \\ + \exp[j2\pi (f_0 + f_m) t] \\ + \exp[j2\pi (f_0 + 2f_m) t] \end{Bmatrix}. \quad (4)$$

With the help of polarization controllers (PC), the output optical fields of MZM_2 and OPS are adjusted with orthogonal polarization. Making sure that the polarization direction of the signal generated by MZM_2 is overlapped to the principle axes x of polarization beam combiner (PBC), leaving the signal generated by OPS with its polarized direction along y. After that a linear polarizer (LP) with its principle polarization direction γ ($\gamma \neq 0^\circ$ or 90°) related to y is employed.

Consequently, the final optical field would be

$$
\begin{aligned}
&E_{out}(t)\\
&= \sin\gamma E_x + \cos\gamma E_y\\
&= -\frac{1}{\sqrt{2}}[A_1\sin\gamma - A_3\cos\gamma]\cdot\begin{Bmatrix}\exp[j2\pi(f_0-f_m)t]\\+\exp[j2\pi(f_0)t]\\+\exp[j2\pi(f_0+f_m)t]\\+\exp[j2\pi(f_0+2f_m)t]\end{Bmatrix}\\
&\quad+\frac{1}{\sqrt{2}}[A_2\sin\gamma - A_4\cos\gamma]\cdot\begin{Bmatrix}\exp[j2\pi(f_0-3f_m)t]\\+\exp[j2\pi(f_0-2f_m)t]\\+\exp[j2\pi(f_0+3f_m)t]\\+\exp[j2\pi(f_0+4f_m)t]\end{Bmatrix},
\end{aligned}
$$

$$
\begin{cases}
A_1 = E_0 J_1(m) J_0(\beta) - E_0 J_1(m) J_2(\beta)\\
A_2 = E_0 J_3(m) + E_0 J_1(m) J_2(\beta)\\
A_3 = E_0 J_1(m)\\
A_4 = E_0 J_3(m).
\end{cases}
\tag{5}
$$

According to (5), the optical sideband suppression ratio (OSSR in dB) between the four inner optical sidebands and the four outer optical sidebands can be calculated as

$$
\begin{aligned}
&OSSR\\
&= 20\log_{10}\left(\frac{A_3\cos\gamma - A_1\sin\gamma}{A_2\sin\gamma - A_4\cos\gamma}\right)\\
&= 20\log_{10}\left\{\frac{J_1(m)\cos\gamma - [J_1(m)J_0(\beta) - J_1(m)J_2(\beta)]\sin\gamma}{[J_3(m) + J_1(m)J_2(\beta)]\sin\gamma - J_3(m)\cos\gamma}\right\}.
\end{aligned}
\tag{6}
$$

It is a function of MI and principle polarization direction. As the MI of MZM_1 (m) and MZM_2 (β) are given, the OSSR will be only dependent on the principle polarization direction (γ). As OSSR over 25dB, the strong four inner optical sidebands with equi-amplitude and same phase direct synthesis of a 4-lines rectangular-shaped OFC. Reference [1] shows such kind of OFC can be used to produce sinc-shaped Nyquist pulses of very high quality and the normalized envelope of the optical field of a rectangular-shaped OFC with N lines and comb spacing Δf can be expressed as

$$
E(t) = \sum_{n=-\infty}^{+\infty} \sin c\left(N\Delta f\left(t - \frac{n}{\Delta f}\right)\right). \tag{7}
$$

It is seen that an ideal way to realize the reconstruction of the pulses is to change the two parameters, N and Δf. However, to achieve adjustable comb lines of an OFC while retaining the original settings of modulator and source in a filterless system is not easy. Fortunately, according to (6), the decrease of the OSSR will naturally make the 4-lines OFC gradually evolved into 8-lines OFC and complete the pulse reconstruction process without changing the parameters of the devices in the filterless system except the LP. This means that the generated Nyquist pulses will have complete reconstruction characteristics, including flexible pulse duration, duty cycle and repetition rate.

III. RESULTS AND DISCUSSIONS

To validate the above analysis, we performed a set of calculations, simulations and experiments. In Fig.2(a), the curves of the power-changing of the four inner optical sidebands (W_2), the four outer optical sidebands (W_1) and the OSSR are given. The parameters of this mode, at f_0 = 193.402THz, were found to be, f_m = 8GHz, m = 0.8, β = 0.58 and γ ranges from 0° to 90°. The accuracy of the analytical results (solid lines) is self-evident. Simulations are realized by building the proposal in the Optisystem 10.0. The small deviation between the analytical model and the simulation (dotted lines) is due to the neglected higher order terms. Considering the phase congruency of the optical sidebands, the feasible sets of parameters γ are marked in pale yellow and mauve. As the parameters γ ranges between 21.9° and 35.5°, the OSSR keeps over 25dB, the overlapping of the two spectra will lead to the generation of a rectangular-shaped OFC with 4 lines. Fig.2(b) and Fig.2(c) show the simulation results of the optical spectra of points P_1 and P_2. The OSSR of the spectra are 56dB and 34.5dB, which are consistent with the numerical analysis.

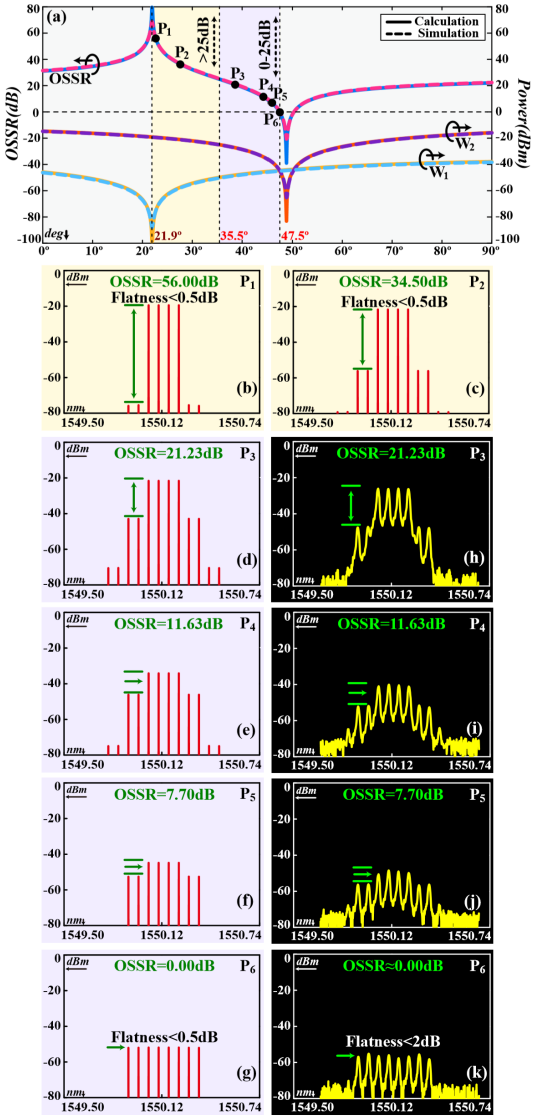

FIGURE 2. (a) The results of the relation between OSSR and γ; (b)-(g) the simulation results of the optical spectra of the points P_1 - P_6; (b) - (g) the experimental results of the optical spectra of the points P_3-P_6.

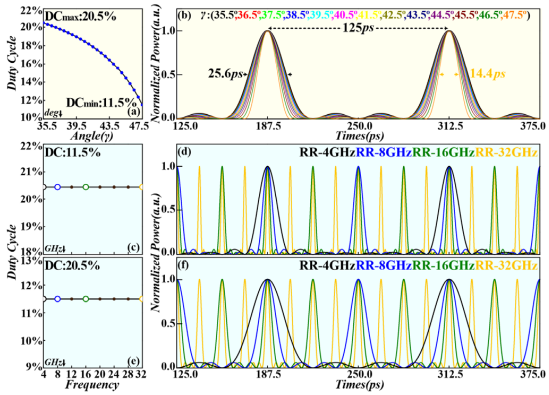

FIGURE 3. The simulation results of the reconstruction process of the final pulses; (a) The relation between duty cycle (DC) of pulses and γ; (b) the corresponding pulses with different duty cycle; (c) - (f) the repetition rate (RR) of pulses changes and corresponding pulses.

Meanwhile, the flatness in Fig.2(b) and Fig.2(c) are below 0.5dB and will be helpful to ensure the quality of the corresponding pulses. Similarly, as the parameter γ varies from 35.5° to 47.5°, the OSSR decreases from 25dB to 0dB, indicating the entering of the region into a new evolutional stage of the OFC. Figs.2(d)-2(e) show the simulation results of the optical spectra of points P_3, P_4, P_5 and P_6 and display the evolution of the OFC. The OSSR of the spectra are 21.23dB, 11.63dB, 7.7dB and 0dB, which is in line with the numerical analysis. As OSSR decreased to 0, the new type of OFC can be formed. There are 8 spectral lines exist in Fig.2(g) and the flatness is below 0.5dB, which constitutes an 8-lines rectangular-shaped OFC. Since we pay more attention to the evolutional stage, the corresponding experiments are carried out and the experimental results are shown in Figs.2(h)-2(k). Considering the requirement of avoiding decorrelation caused by phase fluctuation of carriers and the lack of phase lock installment, in the experiment, the DWL is equivalent to a CW laser and MZM operating in carrier suppression state.

The linewidth of the CW laser, Agilent81600B is 100kHz. The output wavelengths of equivalent DWL are 1550.1 nm and 1550.164 nm, with the power of −7dBm. From the comparison between experimental and simulation results, it is shown that they are basically in agreement, which indicates it is feasible to control the comb lines in our work. Then the pulse duration, duty cycle and repetition rate of the desired pulses have been easily changed by modifying the spectral characteristics of the OFC. Note that, the experimental results also show there are two little drawbacks of the equivalent DWL. One is additional insertion loss results in the decrease of the signal power. The other is the carrier of CW laser which is not completely suppressed will affect the subsequent process of modulation and superposition, resulting in the decrease of signal flatness(<2dB). The two problems can be solved by using a narrow linewidth DWL or a phase locked DWL.

The results of the pulses reconstruction are shown in Fig.3. First, the changes in comb line will directly cause the variation of duty cycle (DC) of the corresponding pulses. This is a continuous process, as presented in Fig.3(a), the DC curve revealed a significant variation due to the different γ. The variation range is from11.5% to 20.5%. Generally, New duty cycle means new pulses, in Fig.3(b) the time-domain waveforms for the different pulses exhibit different property. When the γ increased, the full wave at half maximum (FWHM) of the waveforms reduced from 25.6ps to 14.4ps and the pulse repetition period T equals to 125ps because of the frequency spacing among comb lines is the same as in the previous case, that is f_m = 8GHz. Note that, there are two kinds of sinc-shaped Nyquist pulses with different DC (11.5% and 20.5%) can be obtained in this procedure. Then, we try to change the frequency of driving signal. Tuning the driving frequencies within the widths of intrinsic response curves of the modulators, results in large scanning repetition rate (RR) with different pulse durations. Taking the two kinds of sinc-pulses for example, in figs.3(c) and(e), when the tuning of driving frequencies happens, the linear variation of repetition rates in the range of 4∼40GHz can be clearly observed, which can be used compress and amplify the pico-second pulses with lower distortion as shown in figs.3(d) and 3(f). Note that, theoretically, the tunable range of repetition rate of pulses is confined only by filter bandwidth, since there is no filter built in the scheme, it can be extended easily. On the basis of all above results, it could be deduced that the fitting Nyquist pulses have good reconstruction characteristics.

When it comes to flexibility design, the first word that comes to the mind of designer is sensitivity. Over higher or lower sensitivity is disadvantageous for the practical application of the designs. Generally, there is a best value or variable values for sensitivity, and the latter is more users friendly in practice. Fortunately, the proposed scheme has a very nice feature that will help tune the sensitivity of pulse train reconstruction: the user can determine new layouts for control output by configuring β. According to the formula of OSSR, it can be deduced that the γ lies on β, which can be expressed as

$$\gamma = \arctan\left(\frac{J_1(m) + 10^{\frac{OSSR}{20}} J_3(m)}{10^{\frac{OSSR}{20}} J_3(m) + \left[10^{\frac{OSSR}{20}} J_2(\beta) + J_0(\beta) - J_2(\beta)\right] J_1(m)}\right). \tag{8}$$

assuming the OSSR and m are given, the γ will be only dependent on β. One way to get the trend of γ with a function of β is to take a derivative with respect to β. After that, the γ' can be calculated as

$$\gamma' = \frac{D_1 \cdot D_2}{2[D_3]^2 + 2\{D_4\}^2},$$
$$\begin{cases} D_1 = J_1(m)^2 + 10^{\frac{OSSR}{20}} J_1(m) J_3(m) \\ D_2 = \left(3 - 10^{\frac{OSSR}{20}}\right) J_1(\beta) + \left(10^{\frac{OSSR}{20}} - 1\right) J_3(\beta) \\ D_3 = J_1(m) + 10^{\frac{OSSR}{20}} J_3(m) \\ D_4 = 10^{\frac{OSSR}{20}} J_3(m) + \left[10^{\frac{OSSR}{20}} J_2(\beta) \right. \\ \qquad \left. + J_0(\beta) - J_2(\beta)\right] J_1(m). \end{cases} \tag{9}$$

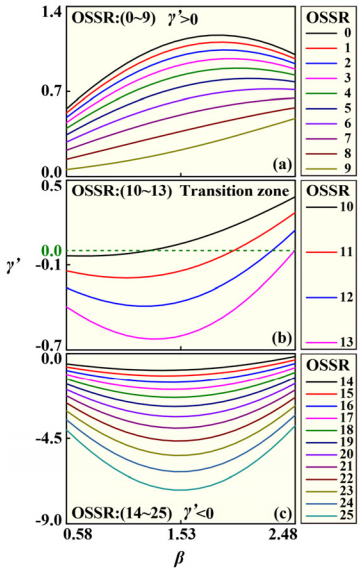

FIGURE 4. (a) The γ' curves vary with β, (a) the range of values for OSSR is 0dB to 9dB and corresponding γ' curves; (b) the range of values for OSSR is 10dB to 13dB and corresponding γ' curves; (c) the range of values for OSSR is 14dB to 25dB and corresponding γ' curves.

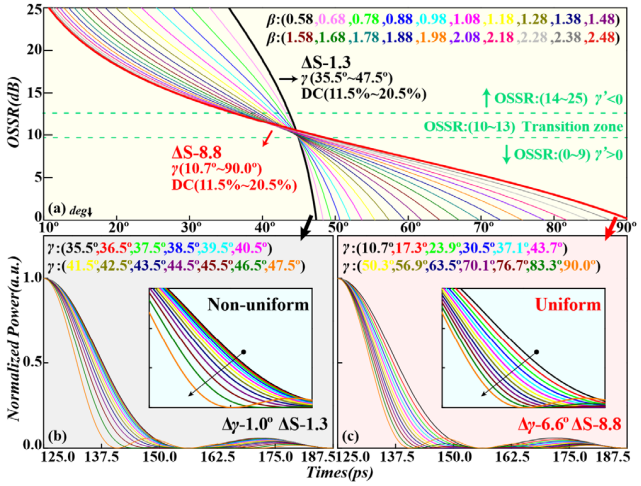

FIGURE 5. (a) The simulation result of the OSSR curves vary with β, (b)–(c) the corresponding pulses reconstruction process.

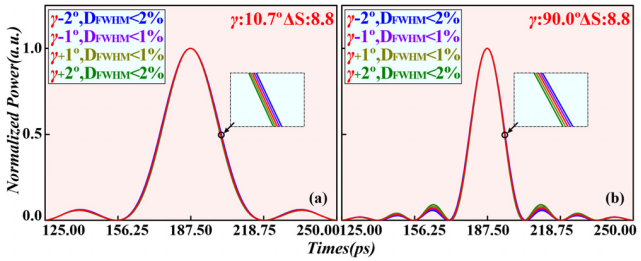

FIGURE 6. (a) The simulation result of the stability of the sinc-shaped Nyquist pulses with FWHM of 25.6ps; (b) The simulation result of the stability of the sinc-shaped Nyquist pulses with FWHM of 14.4ps.

Fig.4 shows the calculation results of the γ' curves vary with β when the range of values for OSSR is 0dB to 25dB. Here, m equals 0.8. In the figure, for a certain OSSR, the γ' varies continuously as the parameter β increasing from 0.58 to 2.48. In Fig.4(a), when OSSR is in the range of 0dB to 9dB, the γ' curve shifts to lower value, but the γ' is plus, indicates the γ increased with the increase of β. While that in Fig.4(c) is not the same, the γ' is minus, proves that as OSSR varies from 14 dB to 25dB, the γ decreased with the increase of β. Meanwhile, in the transition zone between 9dB and 14dB, there is a 0 value in each γ' curves, and the curve shifts as same as the above two group. Considering the functional nature of arctan function, we can make a conclusion that as the β increase, the range of γ has to be expanded to ensure the range of OSSR is 0dB to 25dB, which means the sensitivity of OSSR to γ can be changed by controlling β. The simulation results support the conclusion.

Fig.5 shows the OSSR curves vary with β and the corresponding pulses reconstruction process. In Fig.5(a), the range of γ expanded with the increase of β and its regular is compatible with theoretical analysis. A new variable ΔS is defined based on the γ and DC set up by the function of $(\gamma_{max}\text{-}\gamma_{min})/(DC_{max}\text{-}DC_{min})$, which allows the important property of pulses reconstruction: sensitivity. The results show that the OSSR curves decline rapidly in low MI condition and become smooth and slow while β growing. The initial value of ΔS is 1.3, and the maximum value of ΔS is 8.8 for β ranging in 0.58~2.48. As the value of ΔS increases, the effect of the variation of γ on OSSR decreases, which makes it easy to control the pulse train reconstruction process. This is also illustrated by the results derived from time domain. In fig.5 (b), as $\Delta S = 1.3$, every 1° drop of γ ($\Delta\gamma = 1°$) will cause significant change to the pulse train, and the corresponding pulse envelope is non-uniform distributed, indicates that the reconstruction process has high sensitivity to modifications of the γ. This phenomenon is not shown in fig.5(c), as ΔS increased to 8.8, the jump of $\Delta\gamma$ ($\Delta\gamma = 6.5°$) have no material impact on the above process; instead, the corresponding pulse envelope is almost uniform distributed, means that the sensitivity of reconstruction process is significantly reduced. Contrasting the different reconstruction processes, we could get a conclusion that it is feasible to adjust the sensitivity of the pulses reconstruction by controlling β.

The stability of the pulses while in low sensitivity reconstruction mode is analyzed. In the mode, ΔS equals 8.8. The simulation results are shown in Fig.6. In Fig.6(a), as $\gamma = 10.7°$, sinc-shaped Nyquist pulse with FWHM of 25.6ps can be achieved and exhibited high stability under γ drifts. Consider the maximal angular error of γ is up to 2°. With changing of γ, the pulse is smooth and no obvious distortion, a deviation of $\pm 1°$ will cause an error in FWHM (D_{FWHM}) less than 1%. In Fig.6(b), the narrow sinc-shaped Nyquist pulse with FWHM of 14.4ps also has the important characteristic, which demonstrates that the generator is very flexible, stable and easy to control.

In the optical communication system, the conversion between optical signals and electrical signals is an indispensable process. The quality of photoelectric output signal has a direct impact on the final result of the subsequent

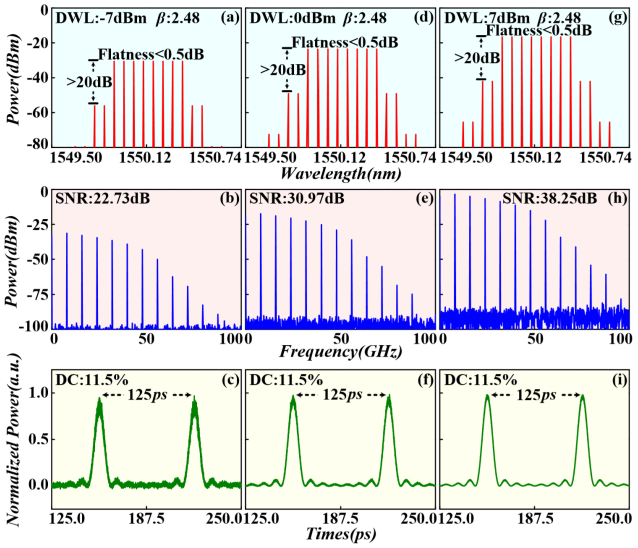

FIGURE 7. The simulation results of photodetection process; (a), (d) and (g), the spectra of input optical signals; (b), (e) and (h), the spectra of output electrical signals; (c), (f) and (i), the corresponding time domain waveforms of output electrical signals.

signal processing. Thus, the effect of the photodetection on the final signal needs to be considered. Since the similarity exists between the photodetection processes of the signals, the 8-lines rectangular-shaped OFC is selected for example. The original signal spectrum is shown in Fig.7(a). The power of DWL is set to −7dB, which is same as that used in Fig.2(g) and Fig.2(k). The β equals 2.48, which is higher than that used in Fig.2. Compare the three figures, it is found that the signal power increases with β increasing and the signal-to-noise ratio (SNR) improves by almost 20dB without significantly impairing the signal quality. This is because as the modulation index (β) of MZM_2 rise, more power distributes in the four outer optical sidebands, thereby reducing the energy loss in the superposition process. Therefore, besides the function of controlling sensitivity, adjusting β can also serve as an indirect method to reduce the influence of evolution process on SNR. Then the original signal is amplified, the gain is about 20dB, and entered into a photodetector. The output electrical signal and corresponding time domain waveforms are shown in Fig.7(b) and Fig.7(c). In the figures, the frequency components are evenly distributed and formed sinc-shaped Nyquist pulses envelope. The minimum power of the pulses is able to return to zero and there is no tilt in the waveforms. Due to the weak power of DWL, the SNR of the signal is 22.73dB, as a result, the pulse is obviously affected by the noise of optoelectronic device. It can be improved by increasing output power of the DWL. In Figs.7(d), 7(e) and 7(f), when the DWL is set to 0dBm, the SNR of the final electrical signal rising up to 8dB, and the fluctuation of the envelope decreased significantly. Similarly, in Figs.7(g), 7(h) and 7(i), as laser power continues to increase, the SNR of the output electrical signal will be further optimized and the pulses will eventually have a near ideal sinc-shaped Nyquist constant envelope, which further proved that the proposed scheme is an effective means for OFC and Nyquist pulses generation.

IV. CONCLUSION

We have demonstrated a reconfigurable OFC and Nyquist pulses generation. It has three advantages: 1) this scheme can realize adjustable comb lines of an OFC while retaining the original settings of modulator and source in a filterless system; 2) this scheme needs no special modulation index, and the MI, β can be used to control the sensitivity of the pulses reconstruction; 3) this scheme can realize the pulse duration, the duty cycle and the repetition rate of the final pulses almost continuously changing. Experiments are carried out to generate a flexible OFC, the comb lines of the OFC can be evolved from 4 lines to 8 lines and the comb spacing of that can be varied from 4GHz to 40GHz. The corresponding temporal Nyquist pulses can have sinc shape and complete reconstruction characteristic. The duty cycle, FWHM and repetition rate of the pulse train could be changed in the ranges of 11.5%∼20.5%, 25.6ps∼14.4ps and 4GHz∼40GHz, respectively. Besides, the above OFC and pulses reconstruction processes with tunable sensitivities, the sensitivity factor ΔS could be adjusted from 1.3 to 8.8, such a range is helpful for user to control the generator. We believe that our device could find applications in microwave photonics and optical communications as a variable multi-wavelength optical source or a reconfigurable optical pulse set with tunable sensitivities.

REFERENCES

[1] M. A. Soto, M. Alem, M. A. Shoaie, A. Vedadi, C.-S. Brès, L. Thévenaz, and T. Schneider, "Optical sinc-shaped Nyquist pulses of exceptional quality," *Nature Commun.*, vol. 4, no. 1, p. 2898, Dec. 2013.

[2] H. Toshihiko, H. Ryoya, W. Jianping, Y. Masato, and N. Masataka, "Single-channel 10.2 Tbit/s (2.56 Tbaud) optical Nyquist pulse transmission over 300 km," *Opt. Express*, vol. 26, no. 21, pp. 27221–27236, 2018.

[3] S. Liu, K. Wu, L. Zhou, L. Lu, B. Zhang, G. Zhou, and J. Chen, "Optical frequency comb and Nyquist pulse generation with integrated silicon modulators," *IEEE J. Sel. Topics Quantum Electron.*, vol. 26, no. 2, pp. 1–8, Mar. 2020.

[4] V. Vercesi, D. Onori, J. Davies, A. Seeds, and C.-P. Liu, "Photonic sampling of broadband QAM microwave signals exploiting interleaved optical Nyquist pulses," in *Proc. Opt. Fiber Commun. Conf.*, 2018, p. M2G.3.

[5] J. Hu, S. J. Fabbri, and C.-S. Brès, "Reconfigurable filter-free sinc-shaped RF photonic filters based on rectangular optical frequency comb," in *Proc. Conf. Lasers Electro-Opt.*, 2018, pp. 1–2.

[6] D. Iosif, L. Cosimo, R. H. B. Kyle, J. T. David, T. R. Graham, J. R. David, and P. Periklis, "Frequency comb generation in a silicon ring resonator modulator," *Opt. Express*, vol. 26, no. 2, pp. 790–796, 2018.

[7] D. Pestov, R. K. Murawski, G. O. Ariunbold, X. Wang, M. Zhi, A. V. Sokolov, V. A. Sautenkov, Y. V. Rostovtsev, A. Dogariu, Y. Huang, and M. O. Scully, "Optimizing the laser-pulse configuration for coherent Raman spectroscopy," *Science*, vol. 316, no. 5822, pp. 265–268, Apr. 2007.

[8] S. Preußler, K. Jamshidi, A. Wiatrek, R. Henker, C.-A. Bunge, and T. Schneider, "Quasi-light-storage based on time-frequency coherence," *Opt. Express*, vol. 17, no. 18, pp. 15790–15798, Aug. 2009.

[9] T. Schneider, K. Jamshidi, and S. Preubler, "Quasi-light storage: A method for the tunable storage of optical packets with a potential delay-bandwidth product of several thousand bits," *J. Lightw. Technol.*, vol. 28, no. 17, pp. 2586–2592, Sep. 1, 2010.

[10] M. Nakazawa, T. Hirooka, P. Ruan, and P. Guan, "Ultrahigh-speed 'orthogonal' TDM transmission with an optical Nyquist pulse train," *Opt. Express*, vol. 20, no. 2, pp. 1129–1140, 2012.

[11] A. Vedadi, M. A. Shoaie, and C.-S. Brès, "Near-Nyquist optical pulse generation with fiber optical parametric amplification," *Opt. Express*, vol. 20, no. 26, pp. B558–B565, 2012.
[12] M. A. Shoaie, A. Mohajerin-Ariaei, A. Vedadi, and C.-S. Brès, "Wideband generation of pulses in dual-pump optical parametric amplifier: Theory and experiment," *Opt. Express*, vol. 22, no. 4, pp. 4606–4619, 2014.
[13] C. He, S. Pan, R. Guo, Y. Zhao, and M. Pan, "Ultraflat optical frequency comb generated based on cascaded polarization modulators," *Opt. Lett.*, vol. 37, no. 18, pp. 3834–3836, Sep. 2012.
[14] M. A. Soto, M. Alem, M. A. Shoaie, A. Vedadi, C.-S. Brès, L. Thévenaz, and T. Schneider, "Generation of Nyquist sinc pulses using intensity modulators," in *Proc. CLEO*, Jun. 2013, pp. 1–2.
[15] J. Wu, J. Zang, Y. Li, D. Kong, J. Qiu, S. Zhou, J. Shi, and J. Lin, "Investigation on Nyquist pulse generation using a single dual-parallel Mach-Zehnder modulator," *Opt. Express*, vol. 22, no. 17, pp. 20463–20472, 2014.
[16] Q. Wang, L. Huo, Y. Xing, C. Lou, and B. Zhou, "Cost-effective optical Nyquist pulse generator with ultra-flat optical spectrum using dual-parallel Mach-Zehnder modulators," in *Proc. Opt. Fiber Commun. Conf.*, 2014, p. W1G.5.
[17] L. Ma, J. Wang, J. Chen, and L. Shang, "Optical sinc-shaped Nyquist pulse generation by using of an intensity modulator in a Sagnac loop," in *Proc. 25th Wireless Opt. Commun. Conf. (WOCC)*, May 2016, Art. no. 7506608.
[18] C. Guo, T. Yang, Z. Lu, C. Ge, and Z. Wang, "Nyquist pulse generator by techniques of frequency synthetization," in *Proc. Terahertz, RF, Millim., Submillimeter-Wave Technol. Appl. X*, Mar. 2017, Art. no. 101030.
[19] Y. Fang, J. Yu, J. Zhang, X. Li, N. Chi, and J. Xiao, "Frequency comb selection enabled flexible all optical Nyquist pulse generation," *Opt. Commun.*, vol. 349, pp. 60–64, Aug. 2015.
[20] S. Preussler, N. Wenzel, and T. Schneider, "Flexible Nyquist pulse sequence generation with variable bandwidth and repetition rate," *IEEE Photon. J.*, vol. 6, no. 4, pp. 1–8, Aug. 2014.

HONGYAO CHEN received the B.E. degree in telecommunication engineering from Zhengzhou University, Zhengzhou, China, in 2011, and the Ph.D. degree in communication and information systems from Beijing Jiaotong University, Beijing, China, in 2018. He is currently a Lecturer with the School of Computer and Communication Engineering, University of Science and Technology Beijing. His research interests include microwave photonics, integrated photonics, fiber optics links and subsystems, and optical communications.

JIANPING WANG, photograph and biography not available at the time of publication.

HUIMIN LU, photograph and biography not available at the time of publication.

TIGANG NING, photograph and biography not available at the time of publication.

LI PEI, photograph and biography not available at the time of publication.

JING LI, photograph and biography not available at the time of publication.